RSC Advances

PAPER

View Article Online
View Journal | View Issue

Cite this: *RSC Adv.*, 2020, **10**, 34466

Controlled preparation of multiple mesoporous CoAl-LDHs nanosheets for the high performance of NO_x detection at room temperature†

Di Wang,[a] Zhi Liu,[a] Ye Hong,[a] Chong Lin,[a] Qingjiang Pan,[a] Li Li*[ab] and Keying Shi*[a]

By fine tuning the metal mole ratio, CoAl-LDHs (CA) with a 2D nanosheet structure were successfully prepared *via* a one-step hydrothermal method using urea as both precipitator and pore-forming agent. The morphology of CA samples shows uniform and thin porous hexagonal nanosheets. In particular, CA2-1, prepared with the 2 : 1 molar ratio for Co and Al, respectively, has the highest surface area (54 m^2 g^{-1}); its average transverse size of platelets is 2.54 μm with a thickness of around 19.30 nm and inter-plate spacing of about 0.2 μm. The sample exhibits a high sensing performance (response value of 17.09) towards 100 ppm NO_x, fast response time (4.27 s) and a low limit of detection (down to 0.01 ppm) at room temperature. Furthermore, CA2-1 shows long -term stability (60 days) and a better selectivity towards NO_x at room temperature. The excellent performance of the fabricated sensor is attributed to the special hexagonal structure of the 2D thin nanosheets with abundant mesopores, where the active sites provide fast adsorption and transportation channels, promote oxygen chemisorption, and eventually decrease the diffusion energy barrier for NO_x molecules. Furthermore, hydrogen bonds between water molecules and OH^- could serve as a bridge, thus providing a channel for rapid electron transfer. This easy synthetic approach and good gas sensing performance allow CoAl-LDHs to be great potential materials in the field of NO_x gas sensing.

Received 18th July 2020
Accepted 26th August 2020

DOI: 10.1039/d0ra06250b

rsc.li/rsc-advances

Introduction

Although there have been considerable substantial achievements in recent years, the development of gas sensors still faces many challenges toward the detection of nitrogen oxides (NO_2, NO) such as low sensitivity and high cost. Several metal oxides, graphene, and organic semiconductors have been used as ubiquitous gas sensors towards different hazardous gases.[1–3] In particular, metal oxides have been given more attention because of their good stability and high sensitivity. To date, various oxides, such as ZnO,[4,5] SnO_2 (ref. 6 and 7) and WO_3,[8,9] are intensively investigated. However, high operating temperature and high cost seriously restrict their wide application.

In recent years, 2D materials have been extensively used in photocatalysis, photoelectric conversion and advanced sensing applications because of their unique properties. There are multiple methods to synthesize 2D materials such as intercalant-assisted thermal cleavage, assisted transport growth, and assisted inverse transport growth.[10–12] As prototypical 2D materials, layered double hydroxides (LDHs) have been a burgeoning area of research due to their advantages, including unique lamellar structure, high stability and low cost.[13,14] Duan *et al.*[15] reported that the reaction of H-acid/LDH could be applied to selectively detect the heavy metal mercury ion. Moreover, the ruthenium complex/LDHs was investigated in electrochemical sensors by the same group.[16] Liu *et al.*[17] explored a ZnO-/$ZnFe_2O_4$-based sensor, which afforded a low response value while detecting triethylamine gas. PS@Co-LDHs were prepared to fabricate a gas sensor for ethanol;[18] however, it showed disadvantages such as complicated preparation conditions and high cost issues. Qin *et al.*[19] used PANI/ZnTi-LDHs effectively as a sensitive sensor towards NH_3 at room temperature; moreover, its detection limit was lowered to 200 ppb. Chlorine-intercalated LDHs were explored to sense five common volatile compounds of different concentrations at RT, and this type of a sensor were found to be unselective.[20] Furthermore, our team has investigated $M^{II}M^{III}$-LDHs in recent years.[21–24] Although many aspects were explored, many problems still remain to be solved, *e.g.*, the complicated preparation process and low sensitivity. The detailed survey along with other references are presented in Table S1.† Therefore, a simple

[a]*Key Laboratory of Functional Inorganic Material Chemistry, Ministry of Education, Key Laboratory of Physical Chemistry, School of Chemistry and Material Science, Heilongjiang University, Harbin, 150080, P. R. China. E-mail: shikeying2008@163.com; Fax: +86 451 86609141*

[b]*College of Advanced Agriculture and Ecological Environment, Heilongjiang University, Harbin, 150080, P. R. China. E-mail: lili1993036@hlju.edu.cn; Tel: +86 451 8660 4920*

† Electronic supplementary information (ESI) available. See DOI: 10.1039/d0ra06250b

preparation route is still required to access LDHs, especially with desirable morphology and good performance.

With the goal of solving the abovementioned issues, a simple one-step hydrothermal method was developed to synthesize CoAl-LDHs materials. A 2D mesoporous nanosheet was successfully fabricated by controlling the urea release and adjusting the molar ratio of Co and Al. Benefiting from its 2D morphology, a high surface area and mesoporous structure, the fabricated CoAl-LDHs sensor exhibits excellent sensing performance toward NO_x at RT. The microstructures and various properties of the representative sample CA2-1 are discussed in detail.

Experimental

Chemicals

All chemical substances used in this experiment were of analytical grade and used without further purification. $Co(NO_3)_2 \cdot 6H_2O$ and $Al(NO_3)_3 \cdot 9H_2O$ and urea were purchased from Xilong Chemical Co., Ltd.

Synthesis of LDHs nanoplates

CoAl-LDHs were synthesized using a simple one-step hydrothermal method. Primarily, $Co(NO_3)_2 \cdot 6H_2O$ (0.117, 0.233, 0.348 g), 0.15 g $Al(NO_3)_3 \cdot 9H_2O$ and 1.7 g urea were added to 40 mL of deionized water for dissolution, and the solution was quickly and continuously stirred for 0.5 h to get a clear and transparent solution. Then, the solution was transferred into 50 mL teflon-lined stainless steel autoclave and hydrothermally heated at 90 °C for 6 h. After naturally cooling down to room temperature, the solution was washed with deionized water and ethanol for several times until neutral, and then dried at 60 °C for 12 h. According to their molar ratios of Co : Al (3 : 1, 2 : 1, 1 : 1), the obtained samples were named as CA3-1, CA2-1, and CA1-1, respectively.

Material characterization

The crystal structures of synthesized samples were characterized using X-ray powder diffraction (XRD) with a D/Max-III B type X-ray diffractometer (Cu-K_α, $\lambda = 0.15406$ nm, 40 kV, 30 mA) at a scanning speed was 5° min^{-1}, and compared with the standard JCPDS card no. 51-0045. An infrared spectrometer (American Perkin Elmer company, model: FT-IR Spectrometer) was used to analyze the composition of samples, and the measured wave number range was between 400 and 4000 cm^{-1}. The regular hexagonal shape and structure of the LDHs samples were observed using scanning electron microscopy (SEM) and transmission electron microscopy (TEM). The surface morphology of the samples was analyzed by a MultiMode8 atomic force microscope of Brooke (Germany). The specific surface area and pore size distribution of samples were tested using TriStarII automatic analyzer (Micromeritics Instrument company). X-ray photoelectron spectrum analyzer was used in this study with a Thermal VG ESCALAB MK250 (1468.4 eV).

Preparation of gas sensitive sensor film

The prepared Au electrode spacing is 20 μm. First, 0.05 g of the prepared LDHs sample was added to 0.1 mL of deionized water, subjected to ultrasonication for 5 min and obtained as a uniform suspended solution. Then, 0.05 mL of the suspended liquid was taken and added on the electrode dropwise through a pipet gun, and then dried for 3 h at 60 °C.

Gas sensor performance tests process

This experiment test was conducted at (25 ± 2) °C at room temperature, and the relative humidity was (25 ± 4)%. The gas sensor's response value $R = R_a/R_g$ was used for calculation, where R_a and R_g represented the sensor resistance of air and target gas injection, respectively. Both response time and recovery time were defined as the time required for the resistance of gas sensor to change by 85% when the sensing element touched the target gas and air, respectively.

Results and discussion

Morphology and structure characterizations

XRD patterns were obtained to investigate the crystal structure and purity of as prepared CoAl-LDHs samples. As shown in Fig. 1a, the diffraction peaks of samples at $2\theta = 11.70°$, 23.66°, 34.66°, 38.79°, 47.00°, 59.70°, 60.95° corresponded to (003), (006), (012), (015), (018), (110), (113) lattice planes (JCPDS card no. 51-0045).[25,26] Compared with those of CA1-1 and CA3-1, the diffraction peaks of CA2-1 at (003) and (006) lattice planes were intense, which indicated that CoAl-LDHs grew in a certain direction during the formation process. Moreover, no other diffraction peaks were observed in XRD, thus demonstrating the high purity of the prepared samples.[27] According to the Bragg's equation, the interlayer spacing (d003 = 0.767 nm) obtained from the diffraction peak of (003) illustrated that there were larger spaces in CoAl-LDHs, which would accommodate more gas molecules[28] and would be helpful for improving the sensitivity of materials.

FT-IR spectrum was used to analyze the types of functional groups of CoAl-LDHs and further confirm the synthesized structures of LDHs (Fig. 1b). The broad absorption peak at 3512 cm^{-1} indicated the stretching vibration of the hydrophilic O–H and interlayer water molecules. The weaker absorption

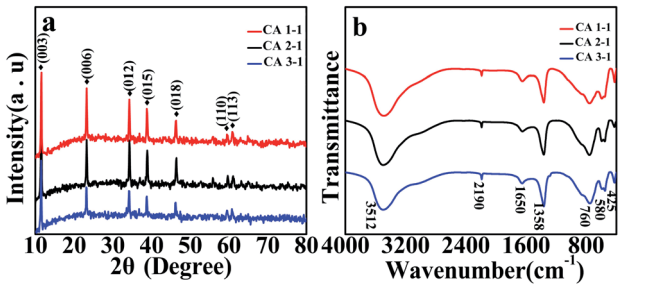

Fig. 1 (a) X-ray diffraction patterns and (b) FT-IR spectra of CA1-1, CA2-1 and CA3-1.

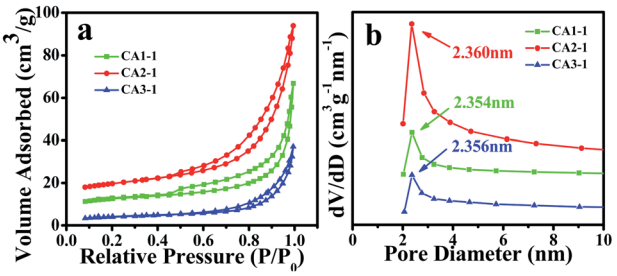

Fig. 2 BET of CA1-1, CA2-1 and CA3-1 samples: (a) specific surface area, and (b) pore diameter distribution curves.

peak at 1650 cm^{-1} belonged to the bending vibration of water molecules between layers.[29] Similarly, the stronger absorption peaks at 1358 cm^{-1} and 760 cm^{-1} corresponded to the bending vibration of CO_3^{2-}, which indicated the successful insertion of CO_3^{2-} into the layer of CoAl-LDHs.[30,31] The peaks at 580 cm^{-1} and 425 cm^{-1} were attributed to the unique bending vibration of the metal oxygen (M–O) bonds.[32] These absorption peaks were a typical characteristic of LDHs absorption peaks and consistent with literature reports. Furthermore, the peak that appeared at ~2190 cm^{-1} was the typical stretching vibration of C≡N bonds in CNO anions, indicating the incomplete decomposition of urea in this process.[33]

Since the adsorption capacity of the target gas was proportional to the specific surface area. The following study was performed using the BET method to test the pore distribution plots of CoAl-LDHs samples. Fig. 2a shows the N_2 adsorption–desorption isotherms of the three samples. All of the CoAl-LDHs nanostructures presented the type IV isotherms and typical H_3 type hysteretic loops. BET specific surface areas of CA1-1, CA2-1 and CA3-1 were approximately 35, 54 and 42 $m^2\ g^{-1}$, respectively. As shown in Fig. 2b, the pore diameter distributions were quite concentrated and distributed around 2.3 nm. This proved that CoAl-LDHs samples have a mesoporous structure and that the mapping of the samples further proved it as shown in Fig. S1.†

Because the morphology is one of the important factors related to the gas sensitivity, the morphology of the synthetic CoAl-LDHs samples was examined by SEM as shown in Fig. 3. Fig. 3a–f show that CA1-1, CA2-1 and CA3-1 presented hexagonal nanosheets with a complete structure and uniform

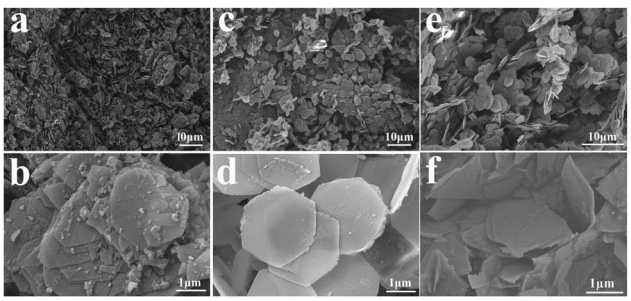

Fig. 3 SEM images of (a and b) CA1-1, (c and d) CA2-1 and (e and f) CA3-1.

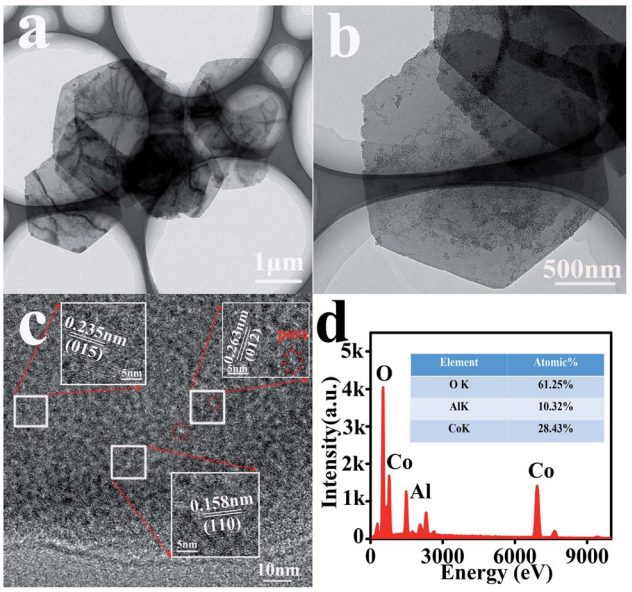

Fig. 4 (a and b) TEM images, (c) HRTEM images and (d) EDS spectra of the CA2-1 sample.

distribution. Interestingly, with the increase of the Co : Al molar ratio, the morphology of LDH became more complete and uniform. Among them, the CA2-1 sample with the optimal ratio of Co : Al = 2 : 1 displayed a relatively perfect hexagonal nanosheet structure (Fig. 3d and 5d), which comprised multiple well-dispersed nanosheets of 19.30 nm. This was beneficial for a better performance due to the increased contact area within the gas molecules. However, when the molar ratio increased to a certain extent, such as in the case of the CA3-1 sample, it showed an abnormal agglomeration phenomenon.

For further confirmation, various characterizations have been performed on the CA2-1 sample. Its TEM and HRTEM

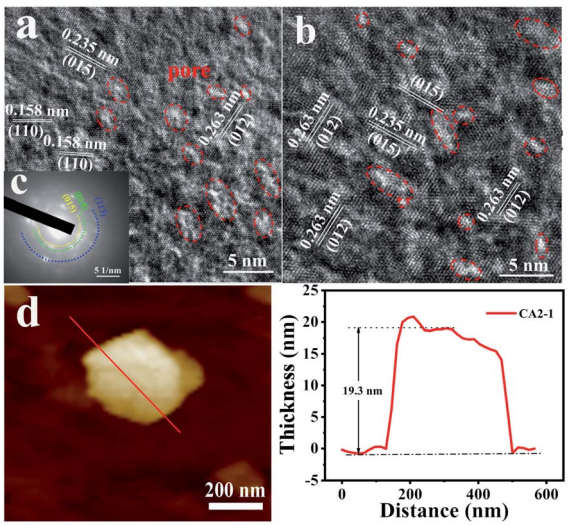

Fig. 5 (a and b) HRTEM images, (c) selected-area electron diffraction (SAED) pattern and (d) AFM images and height profiles of the CA2-1 sample.

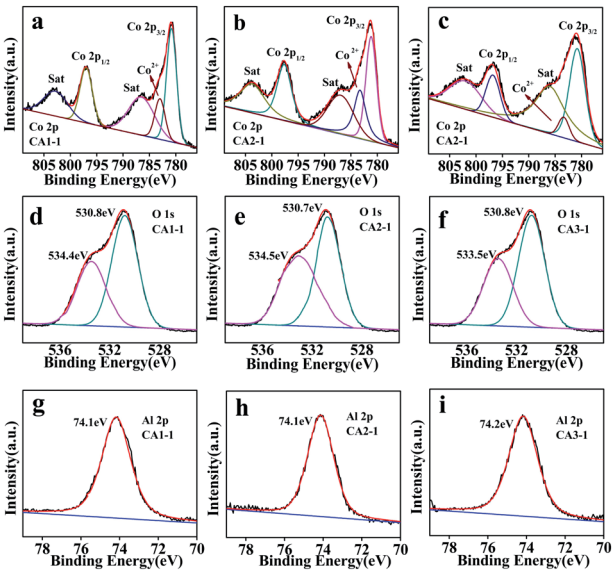

Fig. 6 XPS spectra of CA1-1, CA2-1 and CA3-1 (a–c) Co 2p; (d–f) along with respective O 1s and (g–i) Al 2p.

images are shown in Fig. 4 and 5. As shown in Fig. 4a, the sample presented a clear hexagonal nanosheet structure (Fig. 4b), and there were many 2–5 nm-sized mesopores on the surface of the nanosheets, as shown in Fig. 4c, 5a and b. They were caused by NH_3 and CO_2 produced by urea during the hydrolysis process where the urea molecules acted as pore forming agents. Moreover, the HRTEM image (Fig. 4c and Fig. 5a and b) illustrated that the fringe spacing was 0.263, 0.235 and 0.158 nm, corresponding to the polycrystalline diffraction at (012), (015) and (110) lattice planes. The EDS spectra (Fig. 4d) showed that the atomic element contents of Co, Al and O were 28.43%, 10.23% and 61.23%, respectively. This was accordance with the designed experiment. The SAED pattern confirmed that CA2-1 had a polycrystalline structure (Fig. 5c), and the polycrystalline diffraction rings corresponded to the (015), (118) and (113) lattice planes, which agreed with the results of XRD (Fig. 1a). Moreover, AFM results (Fig. 5d) proved the thickness of the CA2-1 nanosheets was ~19.30 nm.

The compositions of CoAl-LDHs were studied by XPS analysis. The survey spectrum peaks corresponded to Co 2p, O 1s and Al 2p, as shown in Fig. 6. The Co 2p spectra in Fig. 6a–c showed that the two satellite peaks at binding energies of 780.7, 780.8, 780.6 and 797.2, 797.0, 797.4 eV were attributed to Co 2p 3/2 and Co 2p 1/2 of CA1-1, CA2-1 and CA3-1, respectively. This indicated that the Co ion was only presented in the form of Co^{2+}.[34] As shown in Fig. 6d–f, the O 1s spectra of the CoAl-LDHs had two peaks of oxygen species. The peaks atbinding energies of 530.7–530.8 eV were assigned to Al–OH and Co–OH due to the existence of OH between laminates, which provided a large number of binding sites in the sample. Moreover, the binding energies of 533.4–534.5 eV were related to the oxygen vacancy of chemical adsorption.[35,36] As it is known to all, a large number of chemisorbed oxygen vacancies and binding sites could provide more active sites for the adsorption of gas molecules. This was beneficial for improving the gas sensing performance. The fitting results of the O 1s XPS spectra of CA1-1, CA2-1 and CA3-1 samples are listed in Table S5.† Al 2p peaks of CoAl-LDHs shown in Fig. 6g–i indicated that the binding energy at 74.1–74.2 eV manifested the presence of Al^{3+}.[37]

Gas sensing properties

To analyze the gas sensing performance, materials with different mole ratios to NO_x were obtained at RT with 26% RH. Fig. 7a shows the gas response of CA1-1, CA2-1, CA3-1 samples at RT to 100 ppm NO_x. The response of CA2-1 was significantly higher ($R_a/R_g = 17.09$) than those of the other two samples (4.29 and 7.12). The dynamic response and recovery curve of the NO_x gas at different concentrations in CA2-1 presented in Fig. 7b gave further proof of this result. When the sensors were exposed to the target gas, the resistivity rapidly decreased and reached a minimum value in a short time period and stabilized. Similarly, when the sensors exposed to air and drained the NO_x gas, the resistance values quickly returned to the initial value. This indicated that CoAl-LDHs had typical p-type semiconductor characteristics.[38,39] It is clearly seen in Fig. 7c that CA2-1 had the highest response and a short response/recovery time of 4.27/38.93 s to 100 ppm NO_x. The response of the sensor gradually decreased with the decrease in the concentration of NO_x, and the lower detection limit was reached at 0.01 ppm. The dynamic response recovery curve in Fig. 7d demonstrated the excellent recyclability of CA2-1 to 100 ppm NO_x in 10 consecutive cycles.

In practical applications, the sensitive stability is an important parameter for gas sensors. As shown in Fig. 8a, the stability test of CA2-1 to 100 ppm NO_x within 60 days (interval of time is 3 days) was performed. The gas sensor represented the long-term stability at RT, and the sensitivity was basically around 17, indicating that CA2-1 sample would be a beneficial material as a NO_x gas sensor.

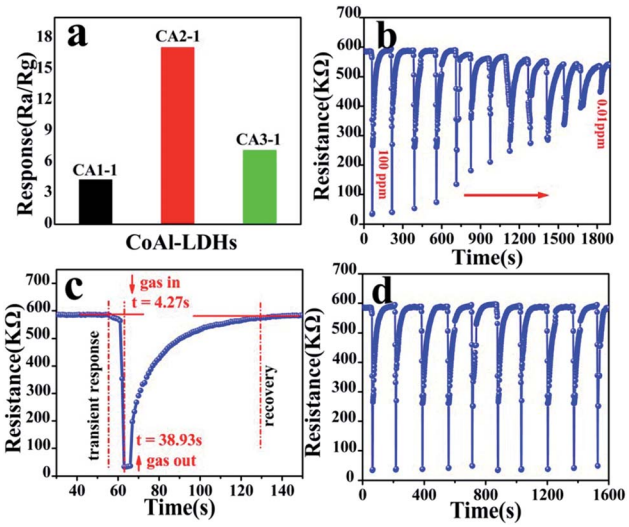

Fig. 7 Gas sensitivity of (a) different ratio CoAl-LDHs samples to 100 ppm NO_x, (b) CA2-1 to 100–0.01 ppm NO_x, (c) response–recovery to 100 ppm NO_x and (d) CA2-1 response to 100 ppm NO_x.

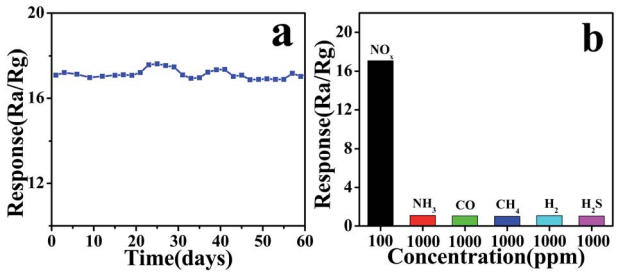

Fig. 8 CA2-1 simple (a) stability (60 days) for 100 ppm NO_x and (b) selectivity for different gas concentrations.

Furthermore, the CA2-1 sensor exhibited good selectivity towards NO_x compared to other tested gases (NH_4, CO, CH_4, H_2, and H_2S), as shown in Fig. 8b.

Discussion of the formation and gas sensing mechanism

The formation and gas sensing mechanism of hexagonal nanosheet CoAl-LDHs was explained as in Scheme 1. In the formation process, urea played a role in the precipitation and pore formation during the synthesis of LDHs. When the hydrothermal temperature increased, urea was gradually hydrolyzed into NH_4^+, CO_2 and OH^- (see eqn (1) and (2)). The precursor solution gradually became alkaline and provided a good condition for the molding of LDHs, as shown in Scheme 1b. In this reaction system, the pH of precipitation Al^{3+} (pH = 3.8) was much lower than that of Co^{2+} (pH = 7.2).[40–42] Therefore, in the first stage, Al ions would react with OH^- (hydrolyzed product of urea) to form amorphous $Al(OH)_3$ and AlO_2^-. This was proved in the above characterization by XRD in which there were no corresponding diffraction peaks of aluminum hydroxide, and thus AlO_2^- and OH^- was produced $[Al_{13}{}^-(OH)_{32}(H_2O)]^{7+}$. Accompanying by a further pH increase, Co^{2+} (pH = 7.2) gradually hydrolyzed to generate $Co(OH)_2$. Along with the reaction progression, Co^{2+} would gradually be replaced by the lamellar structure of Al^{3+} which resulted in the formation of CoAl-LDHs.[43,44] The reaction process is described as follows:

$$H_2NCONH_2 + H_2O \rightarrow 2NH_3 + CO_2 \quad (1)$$

$$NH_3 + H_2O \rightarrow NH_4^+ + 2OH^- \quad (2)$$

$$AlO_2^- + OH^- \rightarrow [Al_{13}{}^-(OH)_{32}(H_2O)]^{7+} \quad (3)$$

As shown in Scheme 1e, there were four absorption peaks close to 3436, 1515, 1361 and 786 cm^{-1} after the adsorption of NO_x (after the NO_x detection for 2 h at RT), which were the

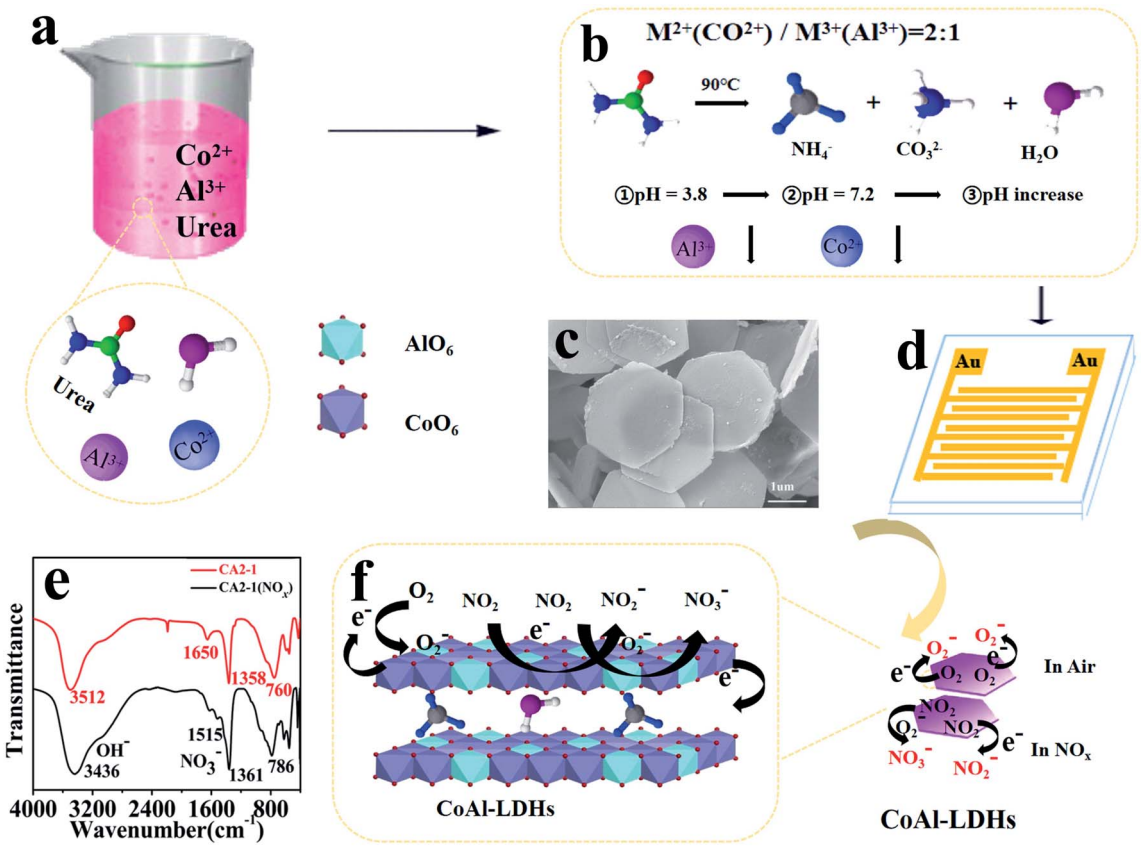

Scheme 1 The formation and gas-sensing mechanism of the 2D nanosheet structure of CoAl-LDHs. (a) Reaction beaker, (b) process of reaction, (c) two-dimensional (2D) nanosheet structure of CA2-1, (d) Au electrode, (e) FT-IR spectra of CA2-1 before and after adsorption of NO_x (test for 2 h), and (f) LDH assembly structure.

stretching modes of OH^- and NO_3^-, respectively. After adsorption, the NO_x molecules trapped electrons from the donor sites of CA2-1, and the hole density became higher while the resistance decreased. This result improved the sensitivity of the sensor. When the sensor was exposed to air, oxygen could easily be adsorbed on its outer surface layers, and easily diffused into the pores of CA2-1, thus capturing the free electrons to form chemically adsorption oxygen, reducing the conductivity of the materials, and placing them in a state of high resistance.[45] Similarly, when the sensor was exposed to NO_x gas, it could capture free electrons directly from the sensor surface to form NO^-/NO_2^- and react with O_2^- to form NO_2^-/NO_3^-, which would eventually increase the hole density on the surface and rapidly reduce the resistivity (Scheme 1f).[46] The reaction equation on the surface of the sensor is described as follows (see eqn (4)–(6)):

$$O_2 + e^- \rightarrow O_2^- \quad (4)$$

$$NO_2 + e^- \rightarrow NO_2^- \quad (5)$$

$$NO_2 + O_2^- + 2e^- \rightarrow NO_3^- + 2O^- \quad (6)$$

Conclusions

CoAl-LDHs with a 2D nanosheet structure were successfully synthesized *via* a simple hydrothermal method using urea as a precipitator and pore-forming agent. An interesting morphology of the samples was obtained by adjusting and tuning the molar ratio of Co and Al. Among them, CA2-1 (Co : Al = 2 : 1) is the optimal one, featuring 2D nanosheets with plenty of mesopores. It presented the best sensitive performance toward NO_x at RT, *i.e.*, higher response value, faster response/recovery time, and lower detection limit. The excellent gas-sensing performance of CA2-1 relative to those of CA1-1 and CA3-1 is summarized as follows: (1) the larger surface area of CA2-1 (54.36 $m^2 g^{-1}$) increased the surface contact reaction with NO_x molecules; (2) unique mesoporous structure, which provided much more adsorption active sites; and (3) the hydrogen bonds between water molecules and OH^- served as a connection bridge, which provided a channel for rapid electron transfer, sped up the response time and enhanced the gas sensitive performance. Furthermore, the relevant mechanism for the formation of CoAl-LDHs was proposed. The present work offers a simple synthesis method for the controllable preparation of LDHs materials. This strategy could be extended to other application fields of LDHs.

Conflicts of interest

There are no conflicts to declare.

Acknowledgements

This work was supported by the National Natural Science Foundation of China (No. 21671060; 2167010747); the Program for Innovative Research Team in Chinese Universities (IRT1237); International Cooperation in Science and Technology Projects of China (2014DFR40480); Applied Technology Research and Development Program Foreign Cooperation Project of Heilongjiang Province (WB15C101).

Notes and references

1 S. M. J. Khadem, Y. Abdi, S. Darbari and F. Ostovari, Investigating the effect of gas absorption on the electromechanical and electrochemical behavior of graphene/ZnO structure, suitable for highly selective and sensitive gas sensors, *Curr. Appl. Phys.*, 2014, **14**, 1498–1503.
2 S. T. Navale, D. K. Bandgar, M. A. Chougule and V. B. Patil, Facile method of preparation of PbS films for NO_2 detection, *RSC Adv.*, 2015, **5**, 6518–6527.
3 S. T. Navale, G. D. Khuspe, M. A. Chougule and V. B. Patil, Camphor sulfonic acid doped PPy/α-Fe_2O_3 hybrid nanocomposites as NO_2 sensors, *RSC Adv.*, 2014, **4**, 27998–28004.
4 Y. Gong, X. F. Wu, J. Y. Chen, W. H. Li, N. Han, D. H. Zhang and Y. F. Chen, Enhanced gas-sensing performance of metal@ZnO core–shell nanoparticles towards ppb–ppm level benzene: the role of metal–ZnO hetero-interfaces, *New J. Chem.*, 2019, **43**, 2220–2230.
5 J. F. Chao, Y. H. Chen, S. M. Xing, D. L. Zhang and W. L. Shen, Facile fabrication of ZnO/C nanoporous fibers and ZnO hollow spheres for high performance gas sensor, *Sens. Actuators, B*, 2019, **298**, 126–927.
6 V. Manikandan, I. Petrila, S. Vigneselvan, R. S. Mane, B. Vasile, R. Dharmavarapu, S. Lundgaard, S. Juodkazis and J. Chandrasekaran, A reliable chemiresistive sensor of nickel-doped tin oxide (Ni-SnO_2) for sensing carbon dioxide gas and humidity, *RSC Adv.*, 2020, **10**, 3796–3804.
7 Y. Su, P. Chen, P. J. Wang, J. Ge, S. Hu, Y. X. Zhao, G. Xie, W. J. Liang and P. Song, Pd-loaded SnO_2 hierarchical nanospheres for a high dynamic range H_2S micro sensor, *RSC Adv.*, 2019, **9**, 5987–5994.
8 J. Zhao, M. Q. Hu, Y. Liang, Q. L. Li, X. Y. Zhang and Z. Y. Wang, A room temperature sub-ppm NO_2 gas sensor based on WO_3 hollow spheres, *New J. Chem.*, 2020, **44**, 5064–5070.
9 Z. Y. Zhang, M. haq, Z. Wen, Z. Z. Ye and L. P. Zhu, Ultrasensitive ppb-level NO_2 gas sensor based on WO_3 hollow nanospheres doped with Fe, *Appl. Surf. Sci.*, 2018, **434**, 891–897.
10 J. M. Li, Mass production of graphene-like single-crystalline $NbSe_2$ (004) nanosheets *via* intercalant-assisted thermal cleavage, *Appl. Phys. A*, 2010, **99**, 229.
11 J. M. Li and J. Fang, Anthracene-assisted inverse transport growth and superconductivity at 3.3 K in unsupported ultrathin {110} Nb and {0001} $NbSe_2$ nanoplates, *J. Mater. Chem. C*, 2017, **5**, 9545.
12 J. M. Li, Robust 2D Room-Temperature Dilute Ferrimagnetism Enhancement in Freestanding Ammoniated Atom-Thin [0001] h-BN Nanoplates, *ACS Appl. Mater. Interfaces*, 2017, **9**, 39626.

13 Y. He, R. Wang, C. G. Sun, S. F. Liu, J. X. Zhou, L. X. Zhang, T. F. Jiao and Q. M. Peng, Facile Preparation of Self-Assembled Layered Double Hydroxide Based Composite Dye Films As New Chemical Gas Sensors, *ACS Sustainable Chem. Eng.*, 2019, **7**, 10888–10899.

14 Y. Chen, Z. X. Fan, Z. C. Zhang, W. X. Niu, C. L. Li, N. L. Yang, B. Chen and H. Zhang, Two-Dimensional Metal Nanomaterials: Synthesis, Properties and Applications, *Chem. Rev.*, 2018, **118**, 6409–6455.

15 Z. Y. Sun, L. Jin, S. T. Zhang, W. Y. Shi, M. Pu, M. Wei, D. G. Evans and X. Duan, An optical sensor based on H-acid/layered double hydroxide composite film for the selective detection of mercury ion, *Anal. Chim. Acta*, 2011, **702**, 95–101.

16 B. Zhang, S. X. Shi, W. Y. Shi, Z. Y. Sun, X. G. Kong, M. Wei and X. Duan, Assembly of ruthenium(II) complex/layered double hydroxide ultrathin film and its application as an ultrasensitive electrochemiluminescence sensor, *Electrochim. Acta*, 2012, **67**, 133–139.

17 S. R. Liu, M. Y. Guan and X. Z. Li, Light irradiation enhanced triethylamine gas sensing materials based on ZnO/$ZnFe_2O_4$ composites, *Sens. Actuators, B*, 2016, **236**, 350–357.

18 Y. Y. Li, F. Zhou, L. Gao and G. T. Duan, Co_3O_4 nanosheet-built hollow spheres containing ultrafine neck-connected grains templated by PS@Co-LDH and their ppb-level gas-sensing performance, *Sens. Actuators, B*, 2018, **261**, 553–565.

19 Y. X. Qin, L. P. Wang and X. F. Wang, A high performance sensor based on PANI/ZnTi-LDHs nanocomposite for trace NH_3 detection, *Org. Electron.*, 2019, **66**, 102–109.

20 D. Polese, A. Mattoccia, F. Giorgi, L. Pazzini, L. D. Giamberardino, G. Fortunato and P. G. Medaglia, A phenomenological investigation on Chlorine intercalated Layered Double Hydroxides used as room temperature gas sensors, *J. Alloys Compd.*, 2017, **692**, 915–922.

21 X. Y. Zhang, L. Teng, Y. Liu, Z. Liu, J. L. Xue, M. Ikram, M. ullah, L. Li and K. Y. Shi, 3D flower-like NiZnAl multimetal oxide constructed by ultra-thin porous nanosheets: a long-term and stable sensing material for NO_x at room temperature, *Sens. Actuators, B*, 2019, **300**, 126–899.

22 Y. L. Ge, K. Kan, Y. Yang, L. Zhou, L. Q. Jing, P. K. Shen, L. Li and K. Y. Shi, Highly mesoporous hierarchical nickel and cobalt double hydroxide composite: fabrication, characterization and ultrafast NO_x gas sensors at room temperature, *J. Mater. Chem. A*, 2014, **2**, 4961.

23 H. Wang, J. Gao, Z. Li, Y. Ge, K. Kan and K. Y. Shi, One-step synthesis of hierarchical α-$Ni(OH)_2$ flowerlike architectures and their gas sensing properties for NO_x at room temperature, *CrystEngComm*, 2012, **14**, 6843–6852.

24 H. X. Sun, Z. Y. Chu, D. H. Hong, G. Zhang, Y. Xie, L. Li and K. Y. Shi, Three-dimensional hierarchical flower-like MgAl-layered double hydroxides: Fabrication, characterization and enhanced sensing properties to NO_x at room temperature, *J. Alloys Compd.*, 2016, **658**, 561–568.

25 Z. B. Tian, Q. Y. Li, J. Y. Hou, L. Pei, Y. Li and S. Y. Ai, Platinum nanocrystals supported on CoAl mixed metal oxide nanosheets derived from layered double hydroxides as catalysts for selective hydrogenation of cinnamaldehyde, *J. Catal.*, 2015, **331**, 193–202.

26 Y. B. Dou, S. T. Zhang, T. Pan, S. M. Xu, A. W. Zhou, M. Pu, H. Yan, J. B. Han, M. Wei, D. G. Evans and X. Duan, TiO_2@Layered Double Hydroxide Core–Shell Nanospheres with Largely Enhanced Photocatalytic Activity Toward O_2 Generation, *Adv. Funct. Mater.*, 2015, **25**, 2243–2249.

27 Y. L. Yang, X. L. Yan, X. Y. Hu, R. Feng, M. Zhou and W. L. Cui, Development of zeolitic imidazolate framework-67 functionalized Co–Al LDH for CO_2 adsorption, *Colloids Surf., A*, 2018, **552**, 16–23.

28 C. Jing, X. Y. Liu, H. C. Yao, P. Yan, G. Zhao, X. L. Bai, B. Q. Dong, F. Dong, S. C. Li and Y. X. Zhang, Phase and morphology evolution of CoAl LDH nanosheets towards advanced supercapacitor applications, *CrystEngComm*, 2019, **21**, 4934.

29 L. J. Zhang, X. G. Zhang, L. F. Shen, B. Gao, L. Hao, X. J. Lu, F. Zhang and B. Ding, Enhanced high-current capacitive behavior of graphene/CoAl-layered double hydroxide composites as electrode material for supercapacitors, *J. Power Sources*, 2012, **199**, 395–401.

30 J. H. Fang, M. Li, Q. Q. Li, W. F. Zhang, Q. L. Shou, F. Liu, X. B. Zhang and J. P. Cheng, Microwave-assisted synthesis of CoAl-layered double hydroxide/graphene oxide composite and its application in supercapacitors, *Electrochim. Acta*, 2012, **85**, 248–255.

31 Y. Y. Li, S. P. Wu, Y. Dai, L. Pang, Q. T. Liu, J. Xie and D. Z. Kong, Investigation of sodium stearate organically modified LDHs effect on the anti aging properties of asphalt binder, *Constr. Build. Mater.*, 2018, **172**, 509–518.

32 G. G. Zhang, S. H. Zang and X. C. Wang, Layered $Co(OH)_2$ Deposited Polymeric Carbon Nitrides for Photocatalytic Water Oxidation, *ACS Catal.*, 2015, **5**, 941–947.

33 Y. F. Zhao, Q. Wang, T. Bian, H. J. Yu, H. Fan, C. Zhou, L. Z. Wu, C. H. Tung, D. O'Hare and T. R. Zhang, Ni^{3+} doped monolayer layered double hydroxide nanosheets as efficient electrodes for supercapacitors, *Nanoscale*, 2015, **7**, 7168–7173.

34 F. Peng, H. Li, D. H. Wang, P. Tian, Y. X. Tian, G. Y. Yuan, D. M. Xu and X. Y. Liu, Enhanced Corrosion Resistance and Biocompatibility of Magnesium Alloy by Mg-Al-Layered Double Hydroxide, *ACS Appl. Mater. Interfaces*, 2016, **51**, 35033–35044.

35 S. M. Xu, T. Pan, Y. B. Dou, H. Yan, S. T. Zhang, F. Y. Ning, W. Y. Shi and M. Wei, Theoretical and Experimental Study on $M^{II}M^{III}$-Layered Double Hydroxides as Efficient Photocatalysts toward Oxygen Evolution from Water, *J. Phys. Chem. C*, 2015, **33**, 18823–18834.

36 S. H. Huang, S. J. Liu and J. Y. Uan, Controllable luminescence of a Li–Al layered double hydroxide used as a sensor for reversible sensing of carbonate, *J. Mater. Chem. C*, 2019, **7**, 11191.

37 Z. B. Tian, Q. Y. Li, J. Y. Hou, L. Pei, Y. Li and S. Y. Ai, Platinum nanocrystals supported on CoAl mixed metal oxide nanosheets derived from layered double hydroxides as catalysts for selective hydrogenation of cinnamaldehyde, *J. Catal.*, 2015, **331**, 193–202.

38 Z. Y. Wang, J. T. Li, X. C. Tian, X. P. Wang, Y. Yu, K. A. Owusu, L. He and L. Q. Mai, Porous Nickel–Iron Selenide Nanosheets as Highly Efficient Electrocatalysts for Oxygen Evolution Reaction, *ACS Appl. Mater. Interfaces*, 2016, **30**, 19386–19392.

39 D. Y. Deng, X. X. Xing, N. Chen, Y. X. Li and Y. D. Wang, Hydrothermal synthesis of β-$Co(OH)_2$ nanoplatelets: a novel catalyst for CO oxidation, *J. Phys. Chem. Solids*, 2017, **100**, 107–114.

40 D. A. Islam, K. Barman, S. Jasimuddin and H. Acharya, Synthesis of ultrasmall and monodisperse sulfur nanoparticle intercalated CoAl layered double hydroxide and its electro-catalytic water oxidation reaction at neutral pH, *Nanoscale*, 2019, **11**, 7560–7566.

41 S. Das, S. Patnaik and K. M. Parida, Fabrication of a Au-loaded $CaFe_2O_4$/CoAl LDH p–n junction based architecture with stoichiometric H_2 & O_2 generation and Cr(VI) reduction under visible light, *Inorg. Chem. Front.*, 2019, **6**, 94.

42 C. Fang, L. Y. Shi, H. Hu, J. P. Zhang and D. S. Zhang, Rational design of 3D hierarchical foam-like Fe_2O_3@CuO_x monolith catalysts for selective catalytic reduction of NO with NH_3, *RSC Adv.*, 2015, **5**, 11013.

43 P. F. Liu, D. Liu, Y. H. Liu and L. Li, ANTS-anchored Zn-Al-CO_3-LDH particles as fluorescent probe for sensing of folic acid, *J. Solid State Chem.*, 2016, **241**, 164–172.

44 B. Zhang, M. Cheng, G. N. Liu, Y. Gao, L. J. Zhao, S. Li, Y. P. Wang, F. M. Liu, X. S. Liang, T. Zhang and G. Y. Lu, Room temperature NO_2 gas sensor based on porous Co_3O_4 slices/reduced graphene oxide hybrid, *Sens. Actuators, B*, 2018, **263**, 387–399.

45 I. Castellanos and O. Marie, An operando FT-IR study of the NO_x SCR over Co-HFER and Fe-HFER using acetylene as a reducing agent, *Catal. Today*, 2017, **283**, 54–65.

46 D. M. Han, L. L. Zhai, F. B. Gu and Z. H. Wang, Highly sensitive NO_2 gas sensor of ppb-level detection based on In_2O_3 nanobricks at low temperature, *Sens. Actuators, B*, 2018, **262**, 655–663.